I&EC research
Industrial & Engineering Chemistry Research

Article

Cite This: Ind. Eng. Chem. Res. 2019, 58, 3159−3169

pubs.acs.org/IECR

Modeling and Control of Proppant Distribution of Multistage Hydraulic Fracturing in Horizontal Shale Wells

Prashanth Siddhamshetty,[†,‡] Kan Wu,[†,¶] and Joseph Sang-Il Kwon*[,†,‡]

[†]Texas A&M Energy Institute, [‡]Artie McFerrin Department of Chemical Engineering, and [¶]Department of Petroleum Engineering, Texas A&M University, College Station, Texas 77845 United States

ABSTRACT: In shale rock formations, multistage hydraulically fractured horizontal wells with slick water are generally used to enhance the production of shale gas and oil. However, slick water proppant transport in simultaneously growing multiple fractures has not been well studied. Motivated by these considerations, we initially focus on the development of a new high-fidelity model for simultaneously growing multiple fractures to describe the fracture propagation by explicitly accounting for stress shadow effects as well as the proppant transport. The hydrocarbon production rate through these multiple fractures is strongly dependent on the proppant distribution within the fractures. To regulate the distribution of proppant at the end of pumping in simultaneously growing multiple fractures, we propose a model-based pumping schedule. Specifically, we develop a reduced-order model utilizing the simulation data from the above-developed high-fidelity model, which is then used to design a Kalman filter and a model predictive controller (MPC) to estimate unmeasurable states and compute online fracturing fluid pumping schedules, respectively. By utilizing the proposed MPC, we show that the proppant bank height at the end of pumping is uniform across multiple fractures.

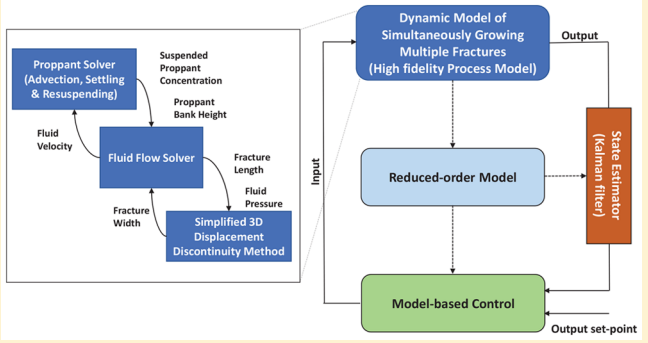

INTRODUCTION

Shale gas and oil are produced from tight shale rock formations with extremely low permeability (10 to 100 nanodarcies).[1] Recent advances in horizontal drilling and hydraulic fracturing technologies have been the game-changer in the petroleum industry and have enabled producing a prolific amount of hydrocarbon from extremely low-permeability shale rock formations. One of the most commonly used completion techniques in unconventional reservoirs for horizontal wells is the plug-and-perforation completion technique. With the use of this technique, multiple isolated fracturing stages are created along the horizontal wellbore from the wellbore toe to the wellbore heel, where in each stage, three to six fractures are generated (Figure 1). Each fracture is created using a cluster of perforations, and typically each perforation cluster consists of 6 to 20 perforations.[2] Specifically, the operation begins by placing a bridge plug to isolate the created fractures, and perforations are generated along the wellbore by firing guns in order to create initial paths for fractures in the current stage. Then, a fracturing fluid is pumped through the perforations at very high-pressure (high enough to overcome the compressive stress of the shale rock formations) to propagate fractures by breaking the shale rock formations. Typically, the fracturing fluid consists of water, proppant (e.g., quartz, sand, silica), and chemical additives. After pumping of the fracturing fluid is stopped, some of the water will leak into the formation from the fracture and the proppant will be trapped inside the fracture during the closure stage. Since the permeability of the propped fractures is high compared to the rock formation, gas and oil will be transported from the shale rock formation to the horizontal wellbore through these created fractures. After generating simultaneously growing multiple fractures within a stage, another stage is created along the horizontal wellbore using the plug-and-perforation completion technique.

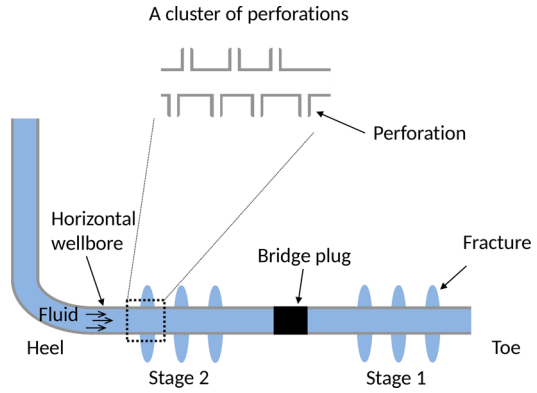

Figure 1. Illustration of multistage hydraulic fracturing operation in a horizontal wellbore.

Received: November 14, 2018
Revised: January 21, 2019
Accepted: January 21, 2019
Published: January 21, 2019

DOI: 10.1021/acs.iecr.8b05654
Ind. Eng. Chem. Res. 2019, 58, 3159−3169

Typically, the spacing between fractures in simultaneously growing multiple fractures is between 10 to 30 m, and the closely spaced fractures often distribute the fracturing fluid unevenly between the fractures resulting in nonuniform fracture geometry.[3,4] Although multistage hydraulic fracturing has resulted in tremendous cost savings by generating simultaneously growing multiple fractures, because of the uneven proppant distribution only 30−40% of the perforation clusters participate in gas and oil production.[5,6] "Stress-shadowing" phenomenon is one of the important contributing factors for the uneven proppant distribution.[7−9] Stress shadow effects refer to additional stresses exerted by an opening fracture on the surrounding rock formation and adjacent fractures. For simultaneously growing multiple fractures, fracturing fluids are distributed into multiple fractures based on pressure drops because of perforation friction, wellbore friction, and fracture propagation. Stress shadow effects exert extra compressional stresses on the interior fractures and due to the increase in flow resistance within interior fractures, the fracturing fluid diverts into the exterior fractures, resulting in nonuniform fracture geometry.

The proppant transport takes place along the horizontal direction by the fracturing fluid and the vertical direction because of the gravitational settling. Specifically, the proppant transport in the horizontal direction is mainly governed by three mechanisms. First, the proppant particles may transport in suspension in a fracturing fluid due to advection. Second, the proppant particles may roll over the surface of a proppant bank. Lastly, the proppant particles on the proppant bank surface may arise due to shear force, and then travel in the horizontal direction before landing on the other proppant bank. In addition to these three mechanisms, the use of slick water may lead to fast proppant settling resulting in the creation of a significant proppant bank at the bottom of fractures, which will influence the subsequent proppant transport mechanism inside the fractures.

In hydraulic fracturing, proppant transport is simulated using two kinds of numerical methods: Eulerian−Lagrangian method and the Eulerian−Eulerian method. In the Eulerian−Lagrangian method, the Lagrangian method is used to solve proppant transport and Eulerian grids are used to solve the fracturing fluid flow.[10−13] This approach is computationally very expensive to be applied to the case of simultaneously growing multiple fractures. Therefore, the Eulerian−Eulerian method was developed to simulate proppant transport and fracturing fluid flow in Eulerian grids. In the following models, proppant transport is simulated using the Eulerian-Eulerian method. Schols and Visser[14] developed a model to determine the proppant bank formation in a vertical fracture by neglecting the fracturing fluid loss. Based on this model, Gu and Hoo[15] proposed a model to simulate the proppant transport with a high-viscosity fracturing fluid. However, they did not consider proppant resuspending. Recently, Hu et al.[16] developed a new model that describes the proppant transport in a single vertical fracture. These proppant transport models focused on simple fracture geometry, that is, a single, planar fracture. While some efforts have been made to describe simultaneously growing multiple fractures under a stress shadow effect, they did not incorporate proppant transport mechanisms.[2,17,18] Motivated by these considerations, the proposed research will develop a new model that accounts for proppant transport as well as simultaneously growing multiple fractures.

The hydrocarbon production rate through multiple fracture networks is strongly dependent on the distribution of proppant within the fractures at the end of hydraulic fracturing operation, because they will create conductive channels for gas and oil transport.[5] Achieving optimal fracture geometry is very important, because even a 10% change in the length of fracture from the optimal value will result in a 50% decrease in gas and oil production rates from shale formations.[19,20] To this end, several studies were conducted recently using real-time model-based feedback control strategies to regulate the uniformity of suspended proppant concentration for conventional reservoirs and proppant bank heights for unconventional reservoirs over the optimal fracture length inside the hydraulic fracture to improve the well productivity;[20−27] however, these studies focused only on a single hydraulic fracture. Recently, we started working on simultaneously growing multiple fractures in multistage hydraulically fractured horizontal wells. One of the important challenges in closely spaced simultaneously growing multiple fractures is that they often result in a nonuniform development of fractures because of stress shadow effects. Stress shadow effects exert extra compressional stresses on the interior fractures and due to the increase in flow resistance within interior fractures, the fracturing fluid diverts into the exterior fractures, resulting in nonuniform fracture geometry. In our recent work,[22] we proposed an optimization-based limited entry fracture design technique to determine the optimal perforation conditions to achieve uniform development of fractures in simultaneously growing multiple fractures by mitigating the stress shadow effects. But the main limitations of our previous work are that (1) we did not consider the proppant transport within the fractures, and (2) the optimization-based limited entry fracture design technique was solved once and offline by utilizing a reduced-order model (ROM); therefore, it may result in poor performance when there are plant-model mismatch, disturbances, or the uncertainties in process model parameters. From a practical standpoint, another challenge in simultaneously growing multiple fractures is achieving uniform proppant distribution and optimal fracture geometry, which is directly related to the gas and oil production rates of stimulated wells. To deal with these two challenges simultaneously, in this work, we will initially develop a high-fidelity model of simultaneously growing multiple fractures to describe the fracture propagation by explicitly accounting for stress shadow effects as well as proppant transport. Then, we will apply optimal perforation conditions obtained from our previous work to the high-fidelity model of simultaneously growing multiple fractures. Lastly, we will focus on developing a new model-based control system by utilizing a ROM of the new high-fidelity model developed in this work, to compute online fracturing fluid pumping schedules to achieve uniform proppant distribution in simultaneously growing multiple fractures. In summary, we will develop a new high-fidelity model and utilize a state-of-the-art model-based control algorithm to achieve a desired fracture geometry and uniform proppant distribution at the end of pumping. In any practical hydraulic fracturing operation, the available real-time measurements are the fracture width near the wellbore and fracture length. Utilizing these available real-time measurements as feedback from the system to design state estimators, in this work, unmeasurable states are predicted, and the plant-model mismatch and the uncertainties in process model parameters are handled.

DOI: 10.1021/acs.iecr.8b05654
Ind. Eng. Chem. Res. 2019, 58, 3159−3169

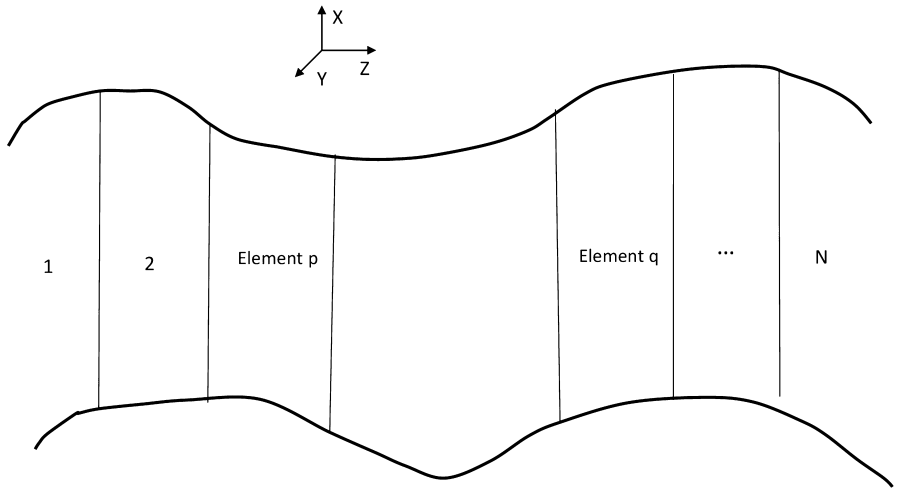

Figure 2. Boundary elements of a fracture.

The rest of the paper is organized as follows: initially, the high-fidelity model of simultaneously growing multiple fractures including proppant transport and proppant resuspending is introduced. This is followed by the section on the development of a ROM utilizing the simulation data from the high-fidelity model, which is then used to design a Kalman filter to estimate unmeasurable states. Lastly, in order to achieve uniform proppant bank height in simultaneously growing multiple fractures at the end of pumping, we presented a model-based feedback controller by mitigating undesired stress shadow effects.

DYNAMIC MODELING OF SIMULTANEOUSLY GROWING MULTIPLE FRACTURES

In this work, a simultaneously growing multiple fracture process is modeled by including: (1) fracture propagation as well as stress shadow effects, (2) proppant transport, and (3) proppant settling and proppant resuspending.

Modeling of Fracture Propagation. Wu and Olson[28] developed the fracture propagation model by including stress shadow effects based on these two main assumptions: (1) fractures cannot propagate to outside of the pay layer, and the height of fractures is constant; (2) all the fractures are vertical, and can generate nonplanar fracture propagation. Pay layer is a reservoir or portion of a reservoir that contains hydrocarbons which can be extracted economically.

Rock Deformation. Stress shadow effects refer to additional stresses exerted by an opening fracture on the surrounding rock formation and adjacent fractures. Stresses at a point (ζ) within an elastic region are integrals of displacement discontinuities, D_i:

$$\sigma_{jk}(\zeta) = \iint_A E_{ijk}(\zeta, \eta) D_i(\eta)\, \mathrm{d}A(\eta) \tag{1}$$

where σ_{jk} is the traction boundary condition, and $E_{ijk}(\zeta, \eta)$ is a tensor field that represents the influence of displacement discontinuities at a point η on the stresses at the point ζ (stress shadow effects). Since it is very hard to obtain analytical solutions for displacement discontinuities, numerical solutions are usually used to solve for displacement discontinuities. In this work, shear, normal, and vertical displacement discontinuities (D_s, D_n, and D_2, respectively) on fracture surfaces are determined using the simplified 3D displacement discontinuity method, which is proposed by Wu and Olson.[28] This method is derived from the fully 3D displacement discontinuity method by neglecting the vertical shear components on the vertical fracture elements, and provides the solution at a fraction of the time that would be required for state-of-the-art techniques.[29,30] In addition, this method accounts for stress shadow effects from nearby fracture elements by considering the 3D mechanical interactions. The shear displacement discontinuity, D_s, induces nonplanar fracture propagation in the fracture-length direction, the normal displacement discontinuity, D_n, represents the fracture opening (fracture width), and D_2 represents the displacement in the vertical direction. The normal and shear displacement discontinuities, D_n^p and D_s^p, respectively, can be determined for given normal and shear stress conditions, σ_s^p and σ_n^p, respectively, which are determined from the fluid flow model, on a fracture element, p, by solving the following set of linear equations:

$$\sigma_s^p = \sum_{q=1}^{M} A_{s,s}^{pq} D_s^q + \sum_{q=1}^{M} A_{s,n}^{pq} D_n^q \tag{2a}$$

$$\sigma_n^p = \sum_{q=1}^{M} A_{n,s}^{pq} D_s^q + \sum_{q=1}^{M} A_{n,n}^{pq} D_n^q \tag{2b}$$

where two different vertical fracture elements are represented using p and q (Figure 2), the total number of vertical fracture elements is represented using M, the normal stress at fracture element p activated by the shear displacement discontinuity at fracture element q is represented by $A_{n,s}^{pq}$, the normal stress at fracture element p activated by the normal displacement discontinuity at fracture element q is represented by $A_{n,n}^{pq}$, the shear stress at fracture element p activated by the shear displacement discontinuity at fracture element q is represented by $A_{s,s}^{pq}$, and the shear stress at fracture element p activated by the normal displacement discontinuity at fracture element q is represented by $A_{s,n}^{pq}$. The matrix A in the simplified 3D displacement discontinuity method is equivalent to tensor field $E_{ijk}(\zeta, \eta)$, which represents the stress shadow effects. The detailed derivation of A is given in ref 28.

Fluid flow. For simultaneously growing multiple fractures, the total injected fracturing fluid and proppant at the wellbore are split into multiple fractures based on pressure drops because of wellbore friction, perforation friction, and fluid

DOI: 10.1021/acs.iecr.8b05654
Ind. Eng. Chem. Res. 2019, 58, 3159−3169

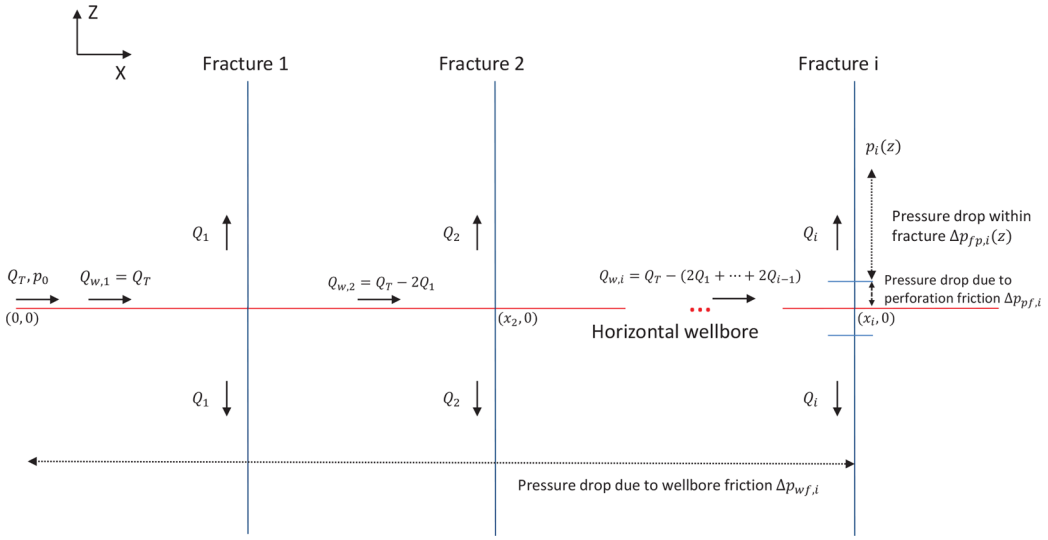

Figure 3. Illustration of the distribution of fracturing fluids into each fracture and the pressure drops because of wellbore friction, perforation friction, and fracture propagation.

pressure within the fractures. The total injected fracturing fluid, Q_{z0}, is equal to the summation of the fracturing fluid injection rates at each fracture, Q_i, which is given by

$$Q_{z0} = \sum_{i=1}^{N} Q_i \tag{3}$$

where N is the number of simultaneously growing fractures (Figure 3).

To satisfy the continuity in pressure along the horizontal wellbore, the pressure at the horizontal wellbore heel, p_o, is equal to the summation of pressure drops because of wellbore friction, $\Delta p_{wf,i}$, perforation friction, $\Delta p_{pf,i}$, fracture propagation, $\Delta p_{fp,i}(z)$, and the pressure at a vertical element of a fracture branch (Figure 3), $p_i(z)$, which is represented as follows:[31]

$$p_o = \Delta p_{wf,i} + \Delta p_{pf,i} + \Delta p_{fp,i}(z) + p_i(z) \tag{4}$$

where the fracture number is denoted using subscript i, and the spatial coordinate in the direction of fracture propagation is denoted by z. The fluid flow through a fracture is modeled using Navier–Stokes equations assuming that the fracture is represented using two smooth parallel surfaces with a constant fracture height, and the pressure drop inside the fracture i due to fluid flow is determined using the following equation:[32]

$$\frac{\partial p_i}{\partial z} = 2^{(n'+1)} k' \left(\frac{1+2n'}{n'}\right)^{n'} H^{-n'} W_i^{-(2n'+1)} Q_i^{n'} \tag{5}$$

where H is the fracture height, W_i is the fracture width, and n' and k' are the fracturing fluid power-law index and consistency index, respectively. The viscosity of fracturing fluid is given by $\mu = k'\gamma^{n'-1}$, where γ is the shear rate. The consistency index parameter, k', is one of the important factors in the viscosity model, and we can compare the viscosity of different fluids by roughly comparing k' values when they have similar power-law expressions. The pressure drop due to wellbore friction, $\Delta p_{wf,i}$, is determined as follows:[32]

$$\Delta p_{wf,i} = 2^{(3n'+2)} \pi^{-n'} k' \left(\frac{1+3n'}{n'}\right)^{n'} D^{-(3n'+1)} \sum_{l=1}^{i} (x_l - x_{l-1}) Q_{w,l} \tag{6a}$$

$$Q_{w,l} = Q_{z0} - \sum_{k=1}^{l-1} 2Q_k \tag{6b}$$

$$Q_{w,l} = Q_{z0} \quad \text{at } l = 1 \tag{6c}$$

where the wellbore diameter is represented using D, the spatial coordinate in the direction of horizontal wellbore is given by x, the fracturing fluid flow rate in fracture k is represented by Q_k, and $Q_{w,l}$ is the fracturing fluid flow rate between two immediate fractures in the horizontal wellbore. The pressure drop due to perforation friction, $\Delta p_{pf,i}$, is calculated for the given number of perforations in each cluster, n_p, and the diameter of each perforation in a cluster, d_p, using the following equation:[31]

$$\Delta p_{pf,i} = \frac{0.807 \rho_{s,i}}{n_p^2 d_p^4 K_d^2} Q_i^2 \tag{7}$$

where $\rho_{s,i}$ is the density of slurry, and K_d is a dimensionless discharge coefficient.

Modeling of Proppant Transport. The proppant volume concentration, C_i, is given by[16]

$$\frac{\partial (C_i W_i)}{\partial t} + \nabla \cdot (W_i C_i V_{p,i}) = 0 \tag{8}$$

where the vector differential operator is denoted by ∇. The net proppant particle velocity inside the fracture, $V_{p,i}$, is determined by describing the proppant transport along the horizontal and vertical directions by the slurry velocity, $V_{hz,i}$, and the settling velocity, $V_{s,i}$, respectively, in the form presented below:[20,21]

$$V_{p,i} = V_{hz,i} + V_{s,i} \tag{9}$$

The gravitational settling velocity of proppant particles in the vertical direction inside the fracture, $V_{s,i}$, is determined by[33]

DOI: 10.1021/acs.iecr.8b05654
Ind. Eng. Chem. Res. 2019, 58, 3159−3169

$$V_{s,i} = \frac{(1 - C_i)^2}{10^{1.82C_i}} \frac{(\rho_p - \rho_f)gD_p^2}{18\mu} \tag{10}$$

where μ is the viscosity of fracturing fluid, ρ_p is the density of proppant, ρ_f is the slick water (pure fluid) density, D_p is the diameter of proppant, and the gravitational acceleration constant is represented by g. The viscosity of fracturing fluid depends on the proppant concentration, C_i, and can be obtained using the empirical model given below:[34]

$$\mu(C_i) = \mu_0 \left(1 - \frac{C_i}{C_{\max}}\right)^{-\beta} \tag{11}$$

where μ_0 is the effective Newtonian viscosity of clean fluid, and β is a constant obtained from experiments, ranging between 1 and 3.[35]

Modeling of Proppant Settling and Proppant Resuspending. Because of the low-viscosity of slick water in unconventional reservoirs, most of the proppant settles quickly to the fracture bottom forming a proppant bank with a height, the value of which is dynamically determined by two factors: the rates of proppant bank formation and proppant resuspending. The proppant bank formation due to the proppant settling can lead to an increase in proppant bank height, and the proppant resuspending due to the shear force can contribute to a decrease in proppant bank height. Therefore, the overall evolution of proppant bank height, $H_{\text{bank},i}$, is described by[16]

$$H_{\text{bank},i} = \int_0^t \left(\frac{dH_{b,i}}{dt} - \frac{dH_{w,i}}{dt}\right) dt \tag{12}$$

where $\frac{dH_{b,i}}{dt}$ is the rate of proppant bank formation, and $\frac{dH_{w,i}}{dt}$ is the rate of proppant resuspending. The formation rate of proppant bank through gravitational proppant settling is described by

$$\frac{dH_{b,i}}{dt} = \frac{C_i V_{s,i}}{C_{\max}} \tag{13}$$

where $C_{\max}$ is the theoretical maximum concentration of proppant bank. The rate of proppant resuspending due to shear force is given by[16]

$$\frac{dH_{w,i}}{dt} = \frac{Kf_i \rho_{s,i} V_{hz,i}}{2\rho_p} \tag{14}$$

where K is the comprehensive experimental factor which is set as 0.8 to obtain a good match with experimental data,[16] f_i is the friction factor of i^{th} fracture, and $V_{hz,i}$ is the slurry velocity. The following expression can be used to compute f_i.[36]

$$\frac{1}{\sqrt{(2f_i)}} = -0.86\left(\frac{(D_p/D_{h,i})}{3.7} - \frac{2.51}{Re_i\sqrt{(2f_i)}}\right) \tag{15}$$

where Re_i is Reynolds number, and $D_{h,i}$ is the hydraulic diameter given by

$$D_{h,i} = \frac{2W_i H_{f,i}}{(W_i + H_{f,i})} \tag{16}$$

where $H_{f,i}$ is the free height for the fracturing fluid flow inside a fracture, which is the distance between the fracture height and the proppant bank height, $(H_{f,i} = H - H_{\text{bank},i})$. Then, Re_i and $\rho_{s,i}$ are obtained by the following equations:

$$Re_i = \frac{\rho_{s,i} V_{s,i} D_{h,i}}{\mu} \tag{17a}$$

$$\rho_{s,i} = (1 - C_i)\rho_f + C_i\rho_p \tag{17b}$$

OPTIMAL FRACTURE GEOMETRY IN UNCONVENTIONAL RESERVOIRS

The section-based optimization method is an offline optimization-based technique for determining the optimum number of wells n_c, the number of fractures per well n_r, and fracture half-length x_f, at which the productivity of a stimulated well is maximized subject to a fixed amount of fracturing resources such as proppant.[37] As illustrated in Figure 4, the

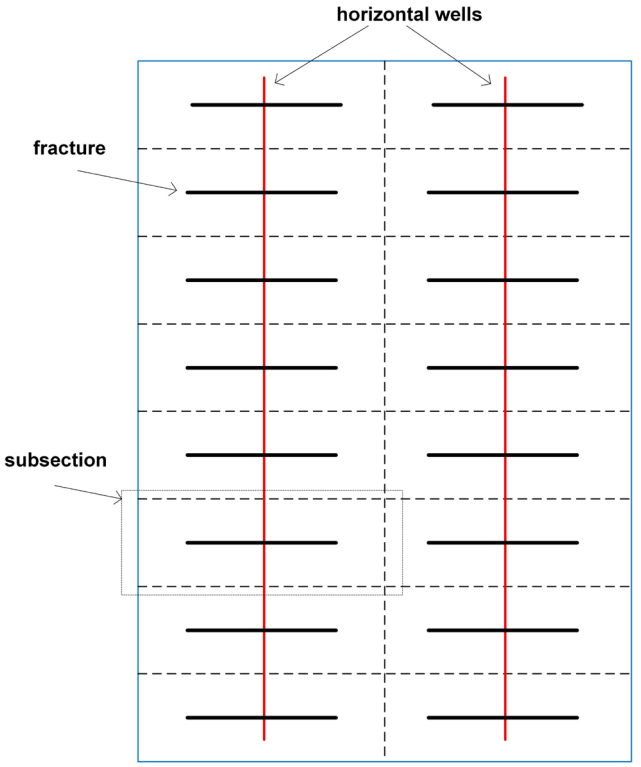

Figure 4. Illustration of a section for the case of two wells $(n_c = 2)$ and eight fractures per well $(n_r = 8)$.

section is the drainage area of an unconventional reservoir, and it is assumed to be a square shape. The section is evenly divided into n_c horizontal wells, and each horizontal well has n_r fractures. The drainage area stimulated by a single hydraulic fracture is called the subsection. Assuming constant values for reservoir properties, such as reservoir permeability, k, the volume factor of formation, B, and the oil viscosity, μ_{oil}, the section productivity is given by

$$J = \frac{2\pi kH}{B\mu_{\text{oil}}} n_f J_{D,f}(A_r, I_x) \tag{18}$$

where $n_f = n_c n_r$ is the aggregate number of fractures created in a section, and J_{Df} is the dimensionless productivity index (PI) for each fracture (i.e., a subsection), which is a function of the aspect ratio, $A_r = x_e/y_e$, and the penetration ratio, $I_x = x_f/x_e$, of a

DOI: 10.1021/acs.iecr.8b05654
Ind. Eng. Chem. Res. 2019, 58, 3159−3169

subsection, where x_e and y_e are the half-width and half-length of a subsection, respectively.

In this work, we assumed the total amount of proppant available to stimulate a section is $M_{prop} = 3.96 \times 10^7$ kg. With this amount of proppant, the optimal values that maximize the productivity from a section are found to be $n_c = 6$, $n_r = 55$, $x_f = 120$ m, and $I_x = 0.895$. More details regarding how to apply the method to hydraulic fracturing can be found in ref 20.

Figure 5 illustrates the proppant bank development and propagation over the course of a hydraulic fracturing process.

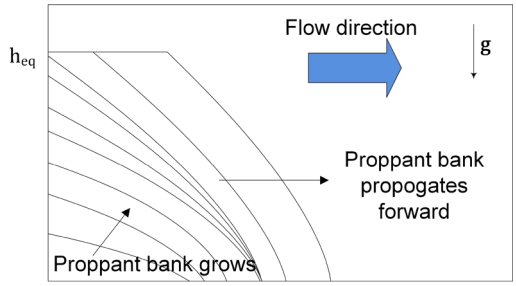

Figure 5. Growth and propagation of proppant bank during hydraulic fracturing.

Because of predominantly low-viscosity fracturing fluids used in unconventional reservoirs, the proppant settles quickly. The settled proppant forms a bank, and after some time the proppant bank formation rate due to gravitational proppant settling will be equal to the proppant resuspending rate due to shear force leading to an equilibrium height, h_{eq}. The main objective of hydraulic fracturing is to achieve a proppant bank height of h_{eq} and a fracture length of x_f. These objectives can be translated into achieving an average width of $W_{avg,target}$, which can be obtained as follows:

$$W_{avg,target} = \frac{M_{prop,frac}}{2\rho_p h_{eq} x_f (1-\phi)} \tag{19}$$

where the amount of proppant to be injected into each fracture is $M_{prop,frac} = 72\,000$ kg, proppant bank porosity is $\phi = 0.54$, and the equilibrium height of proppant bank for the considered flow condition is $h_{eq} = 57$ m. In our case, the calculated target width for each fracture at the end of pumping is $W_{avg,target} = 3.74$ mm. In the following section, we focus on the design of a model predictive controller (MPC) whose objective is to achieve an average fracture width of $W_{avg,target} = 3.74$ mm. In simultaneously growing multiple fractures, close spacing between neighboring fractures often results in a nonuniform development of fractures because of the stress shadow effects. In our previous work, we proposed an optimization-based limited entry fracture design technique to mitigate stress shadow effects.[22] For simultaneously growing multiple fractures, fracturing fluids are distributed into multiple fractures based on pressure drops because of perforation friction, wellbore friction, and fracture propagation. We can achieve equal distribution of fracturing fluids into simultaneously growing multiple fractures by creating a uniform pressure drop in each fracture, which will result in a uniform fracture length. Specifically, we considered one of the widely used multiple hydraulic fracturing techniques called the limited entry fracture design technique; that is to manipulate the pressure drop in each perforation cluster by varying the perforation conditions such as diameter of perforations, and the number of perforations to mitigate stress-shadow effects. First, we developed a model order-reduction technique by integrating the analytical models to calculate the pressure drop due to perforation friction and wellbore friction, and a data-based ROM that accounts for the pressure drop along the fractures due to stress shadow effects. Then, we developed a model-based design technique by utilizing the integrated ROM and the limited entry design technique to compute the optimal perforation conditions which will drive the system to achieve uniform growth of simultaneously propagating multiple fractures by creating an equal amount of pressure drop in each fracture while mitigating the undesired stress shadow effects. We employed the values of $n_p = 12$ and $d_p = 0.011$ m, which was already obtained from our previous work.

MODEL PREDICTIVE CONTROL FOR MULTISTAGE HYDRAULIC FRACTURING

In this section, we first develop a ROM of hydraulic fracturing using simulation data from the above-described high-fidelity model of simultaneously growing multiple fractures, using the multivariable output error state-space (MOESP) algorithm. Then, we assume that the width at the horizontal wellbore (can be determined using pressure data from horizontal wellbore), and the fracture length (can be obtained from microseismic data) are measurable in real-time at every sampling time,[38] which are then used along with the ROM to develop a Kalman filter to estimate unmeasurable variables such as the average width of multiple fractures at each sampling time. Then, we develop an MPC to obtain the optimal pumping schedule required to achieve the desired average fracture width at the end of pumping. As mentioned earlier, achieving the desired average fracture width will lead to the desired proppant bank height as well as the fracture length, which can be translated into the maximum gas and oil production rates.

Reduced-Order Models. Due to the large computational requirement of a dynamic model of simultaneously growing multiple fractures, eqs 2−17, we seek a computationally efficient ROM to design an MPC. First, we obtain input−output data of proppant transport from the dynamic model of simultaneously growing multiple fractures by applying a series of step inputs. Using the MOESP algorithm and the collected simulation data, we obtain a linear time-invariant state-space model of the following form:[39]

$$\underbrace{\begin{bmatrix} x_1(t_{k+1}) \\ \vdots \\ x_n(t_{k+1}) \end{bmatrix}}_{X(t_{k+1})} = A \underbrace{\begin{bmatrix} x_1(t_k) \\ \vdots \\ x_n(t_k) \end{bmatrix}}_{X(t_k)} + B \underbrace{\begin{bmatrix} Q_{z0}(t_k) \\ C_0(t_k) \end{bmatrix}}_{U(t_k)} \tag{20}$$

DOI: 10.1021/acs.iecr.8b05654
Ind. Eng. Chem. Res. 2019, 58, 3159−3169

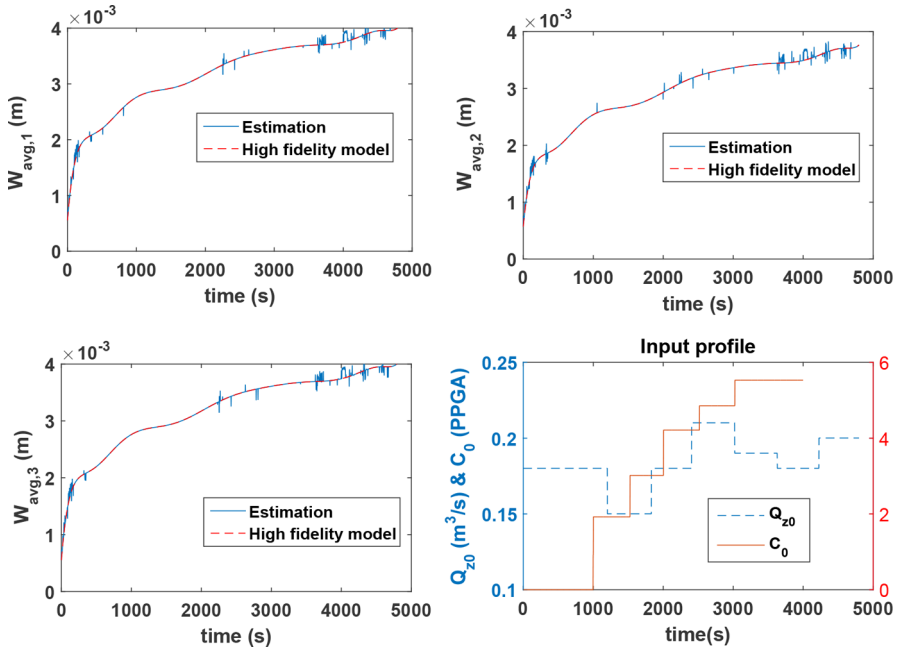

Figure 6. Comparison between the true values and the estimates of average width profiles of simultaneously growing multiple fractures.

$$\underbrace{\begin{bmatrix} W_{\text{avg},1}(t_k) \\ \vdots \\ W_{avg,N}(t_k) \\ W_{0,1}(t_k) \\ \vdots \\ W_{0,N}(t_k) \\ L_1(t_k) \\ \vdots \\ L_N(t_k) \end{bmatrix}}_{Y(t_k)} = C \underbrace{\begin{bmatrix} x_1(t_k) \\ \vdots \\ \\ \\ \\ \\ \\ x_n(t_k) \end{bmatrix}}_{X(t_k)} \tag{21}$$

where the vector of input variables is denoted by $U(t_k)$, $Y(t_k)$ denotes the vector of output variables, and $X(t_k)$ represents the states of ROM. Specifically, $Q_{z0}(t_k)$ is the flow rate and $C_0(t_k)$ is the proppant concentration at the wellbore, $W_{avg,i}(t_k)$ is the average width of fracture i, $W_{0,i}(t_k)$ is the width at the horizontal wellbore of fracture i, $L_i(t_k)$ is the length of fracture i, and $A \in \mathbb{R}^{n\times n}$, $B \in \mathbb{R}^{n\times 2}$ and $C \in \mathbb{R}^{3N\times n}$ are computed by applying the MOESP algorithm to the collected simulation data, U and Y. In the field, available measurements in real-time are the width of fracture at the horizontal wellbore and length of simultaneously growing multiple fractures at every sampling time. These available measurements are then used within a Kalman filter for estimating the average width of simultaneously growing multiple fractures, which is given in the following section.

Kalman Filter Design. The Kalman filter is presented in the following form after combining the prediction and measurement update steps:

$$\hat{X}(t_{k+1}) = A\hat{X}(t_k) + BU(t_k) + M(t_k)(Y_m(t_k) - \hat{Y}(t_k)) \tag{22a}$$

$$M(t_k) = P(t_k)C^{\mathrm{T}}(R(t_k) + CP(t_k)C^{\mathrm{T}})^{-1} \tag{22b}$$

$$P(t_{k+1}) = (I - M(t_k)C)P(t_k) \tag{22c}$$

where Q and R are process and measurement noise covariance matrices, respectively, the estimated unmeasurable variables are denoted using the notation $\hat{(\cdot)}$, $M(t_k)$ is the Kalman filter gain, $P(t_k)$ denotes the covariance of the state estimation error, and $Y_m(t_k) = [W_{0,1}(t_k) \ldots W_{0,N}(t_k), L_1(t_k) \ldots L_N(t_k)]^{\mathrm{T}}$ is a vector of the widths at the horizontal wellbore and the lengths of simultaneously growing multiple fractures (available measurements).

Figure 6 shows that the estimated values of the average width of fractures using the proposed Kalman filter quickly converges to the true values computed from the dynamic model of simultaneously growing multiple fractures.

MPC Formulation. After constructing the ROM and Kalman filter, we design the following MPC to compute an optimal pumping schedule to achieve the desired average width of simultaneously growing multiple fractures (i = 1, ⋯, N):

$$\min_{\substack{C_{\text{stage},k},\ldots,C_{\text{stage},8} \\ Q_{\text{stage},k},\ldots,Q_{\text{stage},8}}} \sum_{i=1}^{N} (\hat{W}_{\text{avg},i}(t_f) - W_{\text{avg,target}})^2 \tag{23a}$$

s.t.

$$\text{Kalman filter, eq (22)} \tag{23b}$$

$$\text{ROM, eqs (20) and (21)} \tag{23c}$$

$$\hat{W}_{0,i}(t_k) = W_{0,i}(t_k), \quad \hat{L}_i(t_k) = L_i(t_k) \tag{23d}$$

$$C_{\text{stage},k-1+m} \le C_{\text{stage},k+m} \le 5\text{PPGA} \tag{23e}$$

$$Q_{\min} \le Q_{\text{stage},k+m} \le Q_{\max} \tag{23f}$$

$$m = 1, \ldots, 8 - k \tag{23g}$$

DOI: 10.1021/acs.iecr.8b05654
Ind. Eng. Chem. Res. 2019, 58, 3159−3169

$$\Delta\left(\sum_{k=1}^{8} 2Q_{\text{stage},k}C_{\text{stage},k}\right) = NM_{\text{prop,frac}} \tag{23h}$$

where N is the total number of simultaneously growing fractures, $W_{\text{avg,target}}$ is the desired value of average fracture width at the end of pumping, $\hat{W}_{\text{avg},i}(t_k)$ is the predicted average width of fracture i using Kalman filter, eq (22), t_f is the total treatment time of hydraulic fracturing, t_k is the current hydraulic fracturing treatment time, Δ is the time duration of each pumping-stage, which is also equal to the sampling time, measurements of $W_{0,i}(t_k)$ and $L_i(t_k)$ are available at $t = t_k$, and $Q_{\text{stage},k}$ and $C_{\text{stage},k}$ are the injected flow rate and proppant concentration during the k^{th} pumping stage ($t \in [t_k, t_k + \Delta]$), respectively.

In the above presented optimization problem of eq 23, the objective function, eq 23a, is the overall quadratic deviations of the predicted average widths from the desired value at the end of pumping. The available measurements of fracture length and the fracture width at the horizontal wellbore, eq 23d, are used to initialize the Kalman filter, eq 23b, to predict the unmeasurable average fracture width trajectories of simultaneously growing multiple fractures. Please note that the Kalman filter plays a role as a soft sensor to provide measurements to the MPC formulation. The maximum proppant concentration that can be transported using slick water has been constrained via eq 23e. By considering the available pumping capacity, we impose a constraint of eq 23f on the fracturing fluid flow rate at the wellbore. The constraint of eq 23h describes the total amount of available proppant, which will be injected over the course of the hydraulic fracturing treatment to create N fractures. In multistage hydraulic fracturing, there are two challenges: (1) mitigating stress shadow effects to achieve a uniform fracture growth; (2) driving the average fracture width over multiple fractures to a set-point value, which will result in a uniform proppant bank height in simultaneously growing multiple fractures. We mitigate the stress shadow effects by using the optimal perforation conditions obtained in our previous work.[22] The remaining challenge of regulating the average fracture widths of multiple fractures will be handled by the proposed MPC scheme.

Remark 1. The operation of hydraulic fracturing can be viewed as a "semibatch" process. Similar to a standard "semibatch" reactor, where the partial filling of reactants with the flexibility of adding more as time progresses is allowed, the addition of more fracturing fluid and proppant is allowed. Semibatch processes are finite duration processes with the absence of equilibrium points and time-varying dynamics over a range of operating conditions, and the primary control objective is to reach a specified product quality. Similarly, in hydraulic fracturing, the duration of the operation is prespecified, and the primary control objective is to reach the desired average fracture width at the end of pumping, which will lead to the desired proppant bank height as well as the fracture length at the end of pumping; in particular, these attributes are directly related to the gas and oil production rates of stimulated wells. We considered the entire duration of the hydraulic fracturing as the prediction horizon of MPC. The input variables, $C_{\text{stage},k}$ and $Q_{\text{stage},k}$, are obtained by solving the optimization problem with a shrinking prediction horizon $N_p = t_f - t_k$, and the first step of a series of solutions was applied to the high-fidelity process model in a sample-and-hold fashion. This procedure was repeated at every sampling time until the end of the process, which is analogous to applying an MPC system to a semibatch system.

A CASE STUDY FOR THREE SIMULTANEOUSLY GROWING FRACTURES

In this section, we first presented a base case with three simultaneously growing fractures, which may result in nonuniform propped fracture geometry because of stress shadow effects, leading to poor gas and oil production rates from shale reservoirs. We applied the proposed MPC to regulate the average width of simultaneously growing multiple fractures to a desired fracture geometry. The parameters used in the dynamic model of eqs 2−17 are presented in Table 1.[28]

Table 1. Model Parameters Used for the Base Case Simulation

parameter	symbol	value
fracture spacing	X_{sep}	29.3 m
Young's modulus	E	0.87×10^{10} Pa
Poisson ratio of formation	ν	0.2
density of proppant	ρ_p	2650 kg/m^3
leak-off coefficient	C_{leak}	1×10^{-5} m/s$^{1/2}$
diameter of proppant	D_p	0.001 m
fracture height	H	60 m
fracturing fluid power law index	n'	1
fracturing fluid consistency index	k'	0.01 Pa·s
horizontal wellbore diameter	D	0.1 m
distance from horizontal wellbore heel to the first fracture in each stage	x_1	268 m
dimensionless discharge coefficient	K_d	0.89
minimum horizontal stress	$S_{h,\text{min}}$	6.95×10^7 Pa
maximum horizontal stress	$S_{h,\text{max}}$	7.16×10^7 Pa

Base Case with Nonuniform Propped Fractured Geometry. In the base case, we injected the fracturing fluid with a constant flow rate, 0.18 m^3/s, and a total proppant amount of $3M_{\text{prop,frac}}$ is injected over the course of hydraulic fracturing. We considered 20 perforations per cluster ($n_p = 20$), and the diameter of perforation was $d_p = 0.015$ m. For this case, Figure 7 shows that the exterior fractures were propagated more compared to the interior fracture, while the interior fracture width was greatly restricted. The stress shadow effects exerted additional stress on the interior fracture, and the increased flow resistance diverted the fracturing fluids into the exterior fractures. As a result, the propped fracture geometry of fractures is different from the desired one obtained from the section-based optimization method as shown in Figure 8.

Closed-Loop Simulation Results for Three Simultaneously Growing Fractures under the Proposed MPC. In this subsection, we applied the proposed MPC for the case of three simultaneously growing fractures to regulate the average width, which is highly related to the main objective of achieving uniform proppant bank height across fractures at the end of pumping. To achieve an equilibrium proppant bank height of $h_{\text{eq}} = 57$ m, and an optimal half-length of fracture, $x_f = 120$ m, the desired average fracture width was found to be $W_{\text{avg,target}} = 3.74$ mm. For all the simulations, the pumping time of pure fracturing fluid (pad), t_p, was fixed to be 1200 s, which was found to avoid premature termination of fracture propagation. The proposed MPC system and the Kalman filter were initialized from the beginning of hydraulic fracturing

DOI: 10.1021/acs.iecr.8b05654
Ind. Eng. Chem. Res. 2019, 58, 3159−3169

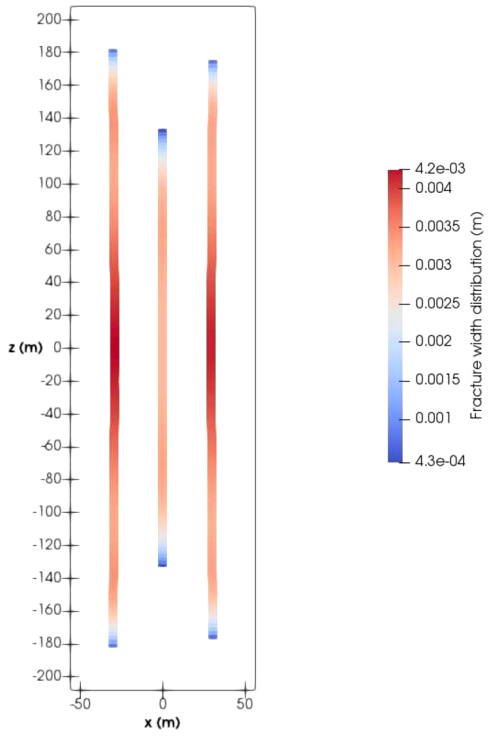

Figure 7. Fracture length and width distributions obtained at the end of pumping for the base case.

operation. The sampling and total treatment times, Δ and t_f, respectively, were fixed as 600 and 4800 s, respectively. In total, we considered eight pumping stages for proppant and fracturing fluid injection.

One of the challenges in closely spaced simultaneously growing multiple fractures is that they often result in a nonuniform development of fractures because of stress shadow effects. In this work, we used an optimization-based limited entry fracture design technique to determine the optimal perforation conditions to achieve uniform development of fractures.[22] Specifically, we considered the conditions of n_p = 12 and d_p = 0.011 m for perforations in each cluster through which we were able to achieve almost uniform distribution of fracturing fluids into simultaneously growing multiple fractures as shown in Figure 9.

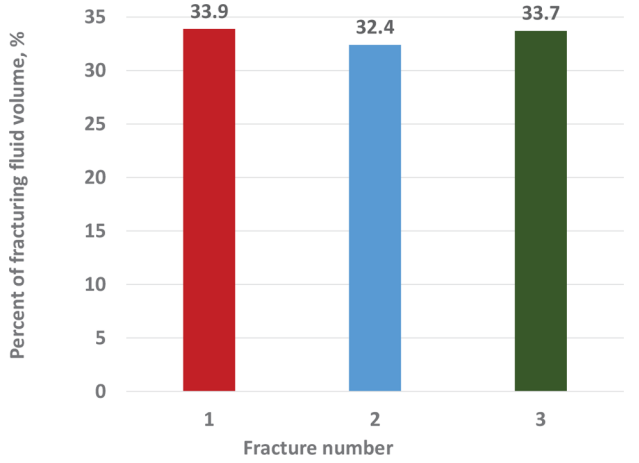

Figure 9. Percentage of the total fracturing fluid volume distributed into each fracture at the end of pumping under the optimal perforation conditions.

Then, we applied the proposed MPC to the dynamic model of simultaneously growing multiple fractures to achieve the desired average fracture width. The average fracture width profiles of the three fractures are presented in Figure 10, where they are close to the desired value at the end of pumping. The computed optimal pumping schedule by the proposed MPC is shown in Figure 11. Since we are able to regulate the average width, the proppant bank height of the simultaneously growing multiple fractures is uniform with the equilibrium value, over the optimal half-length, x_f, as shown in Figure 12. After applying the obtained optimal pumping schedule, still some of the proppant (2000 kg) is in the suspension, which are assumed to quickly join the bank during the shut-in period.

CONCLUSIONS

A MPC system is presented to achieve the uniform proppant bank height across the optimal fracture length in simultaneously growing multiple fractures at the end of pumping. First, we introduced a dynamic model of simultaneously

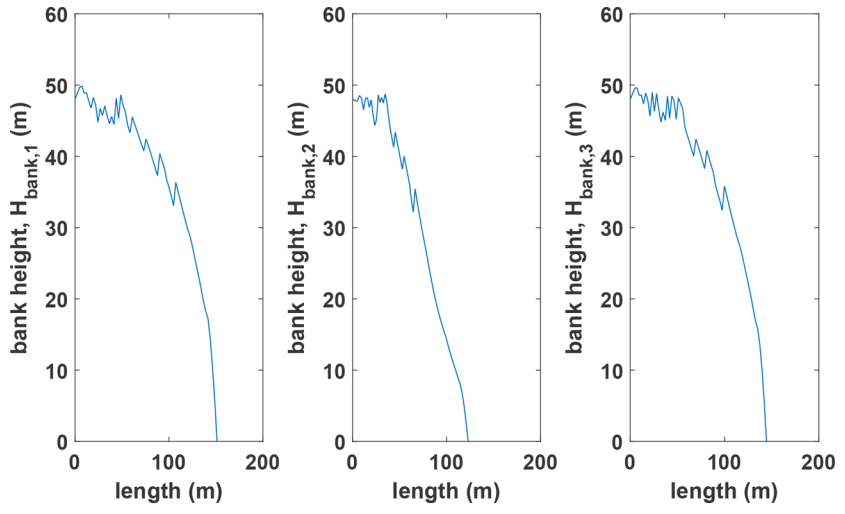

Figure 8. Spatial proppant bank height profiles of the simultaneously growing three fractures obtained at the end of pumping for the base case.

DOI: 10.1021/acs.iecr.8b05654
Ind. Eng. Chem. Res. 2019, 58, 3159−3169

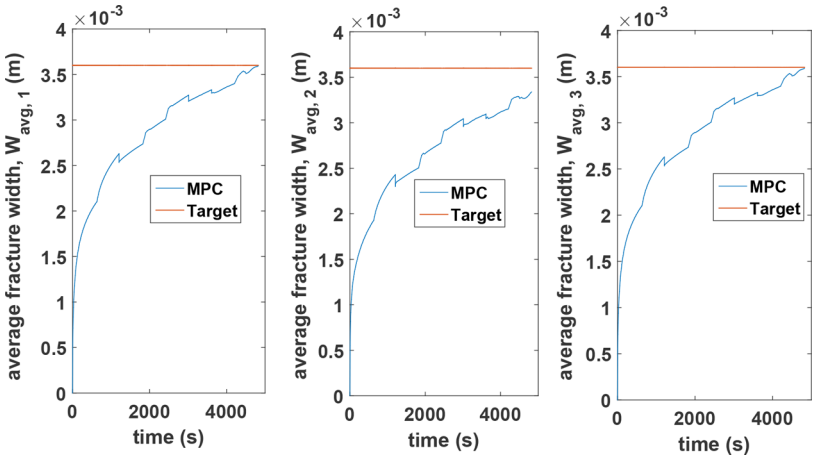

Figure 10. Average width profiles of simultaneously growing three fractures during hydraulic fracturing under the proposed controller.

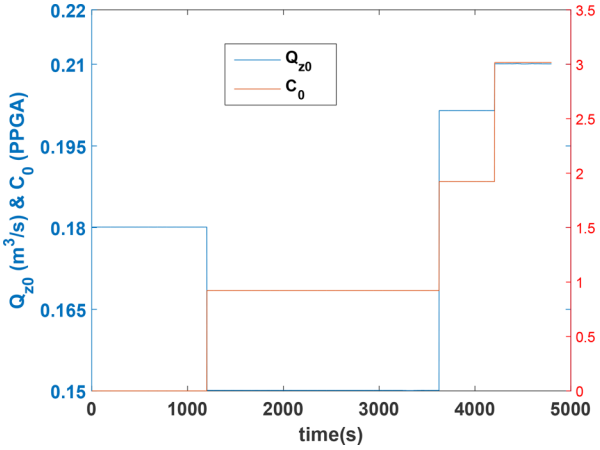

Figure 11. Optimal pumping schedules generated under the proposed controller.

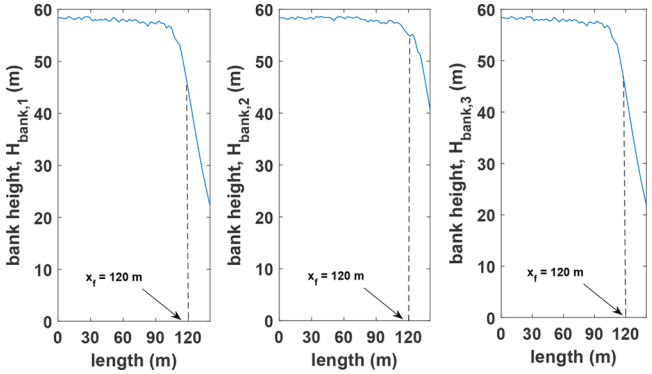

Figure 12. Spatial proppant bank height profiles of the simultaneously growing three fractures obtained at the end of pumping.

growing multiple fractures to describe the formation of a proppant bank including proppant settling and proppant resuspending. Second, we determined the optimal well-fracture configuration by employing the section-based optimization method, which maximizes the overall production of gas and oil from shale formations. Third, a ROM was developed utilizing the simulation data from the dynamic model of simultaneously growing multiple fractures, which is used in the Kalman filter to predict the average width of simultaneously growing multiple fractures. We employed optimal perforation conditions in the dynamic model of simultaneously growing multiple fractures which were available from our previous work to mitigate the stress shadow effects. Lastly, the proposed MPC scheme was applied to compute online fracturing fluid pumping schedules. The proposed methodology was able to generate a uniform proppant bank height along the targeted fracture length while simultaneously incorporating the limitations of actuators, process operational safety, and economic considerations.

AUTHOR INFORMATION

Corresponding Author

*E-mail: kwonx075@tamu.edu.

ORCID

Joseph Sang-Il Kwon: 0000-0002-7903-5681

Notes

The authors declare no competing financial interest.

ACKNOWLEDGMENTS

The authors gratefully acknowledge financial support from the National Science Foundation (CBET-1804407), the Artie McFerrin Department of Chemical Engineering, and the Texas A&M Energy Institute.

REFERENCES

(1) Cipolla, C. L.; Lolon, E. P.; Erdle, J. C.; Rubin, B. Reservoir modeling in shale-gas reservoirs. *SPE reservoir evaluation & engineering* **2010**, *13*, 638−653.

(2) Lecampion, B.; Desroches, J. Simultaneous initiation and growth of multiple radial hydraulic fractures from a horizontal wellbore. *J. Mech. Phys. Solids* **2015**, *82*, 235−258.

(3) Wheaton, B.; Miskimins, J.; Wood, D.; Lowe, T.; Barree, R. Integration of distributed temperature and distributed acoustic survey results with hydraulic fracture modeling: a case study in the Woodford shale. In 2015 SEG Annual Meeting. Society of Exploration Geophysicists (SEG-2015−5830237), 2015, New Orleans, LA.

(4) Wu, K.; Olson, J. E. Mechanisms of simultaneous hydraulic-fracture propagation from multiple perforation clusters in horizontal wells. *SPE Journal* **2016**, *21*, 1000−1008.

(5) Cipolla, C. L.; Mack, M. G.; Maxwell, S. C. Reducing exploration and appraisal risk in low-permeability reservoirs using microseismic fracture mapping. In Canadian Unconventional Resources and International Petroleum Conference (SPE 137437), 2010, Calgary, Alberta, Canada.

(6) Miller, C. K.; Waters, G. A.; Rylander, E. I. Evaluation of production log data from horizontal wells drilled in organic shales. In

DOI: 10.1021/acs.iecr.8b05654
Ind. Eng. Chem. Res. 2019, 58, 3159−3169

North American Unconventional Gas Conference and Exhibition (SPE 144326), 2011, The Woodlands, Texas.
(7) Germanovich, L. N.; Astakhov, D. K.; Mayerhofer, M. J.; Shlyapobersky, J.; Ring, L. M. Hydraulic fracture with multiple segments I. Observations and model formulation. *International Journal of Rock Mechanics and Mining Sciences* **1997**, *34*, 97−e1.
(8) Fisher, M. K.; Heinze, J. R.; Harris, C. D.; Davidson, B. M.; Wright, C. A.; Dunn, K. P. Optimizing horizontal completion techniques in the Barnett shale using microseismic fracture mapping. SPE Annual Technical Conference and Exhibition (SPE 90051), 2004, Houston, Texas. DOI: 10.2118/90051-MS
(9) Meyer, B. R.; Bazan, L. W. A discrete fracture network model for hydraulically induced fractures-theory, parametric and case studies. In SPE hydraulic fracturing technology conference. Society of Petroleum Engineers (SPE 140514), 2011, The Woodlands, Texas.
(10) Tsai, K.; Fonseca, E.; Lake, E.; Degaleesan, S. Advanced computational modeling of proppant settling in water fractures for shale gas production. *SPE Journal* **2013**, *18*, 50−56.
(11) Blyton, C. A.; Gala, D. P.; Sharma, M. M. A Comprehensive Study of Proppant Transport in a Hydraulic Fracture. SPE Annual Technical Conference and Exhibition (SPE 174973), 2015, Houston, Texas.
(12) Zeng, J.; Li, H.; Zhang, D. Numerical simulation of proppant transport in hydraulic fracture with the upscaling CFD-DEM method. *J. Nat. Gas Sci. Eng.* **2016**, *33*, 264−277.
(13) Wu, C. H.; Yi, S.; Sharma, M. M. Proppant distribution among multiple perforation clusters in a horizontal wellbore. In SPE Hydraulic Fracturing Technology Conference and Exhibition (SPE 184861), 2017, The Woodlands, Texas.
(14) Schols, R. S.; Visser, W. Proppant bank buildup in a vertical fracture without fluid loss. In SPE European Spring Meeting (SPE 4834), 1974, Amsterdam, Netherlands.
(15) Gu, Q.; Hoo, K. A. Evaluating the performance of a fracturing treatment design. *Ind. Eng. Chem. Res.* **2014**, *53*, 10491−10503.
(16) Hu, X.; Wu, K.; Song, X.; Yu, W.; Tang, J.; Li, G.; Shen, Z. A new model for simulating particle transport in a low viscosity fluid for fluid driven fracturing. *AIChE J.* **2018**, *64*, 3542−3552.
(17) Wu, K.; Olson, J.; Balhoff, M. T.; Yu, W. Numerical analysis for promoting uniform development of simultaneous multiple-fracture propagation in horizontal wells. *SPE production & operations* **2017**, *32*, 41−50.
(18) Peirce, A.; Bunger, A. Interference Fracturing: Nonuniform Distributions of Perforation Clusters That Promote Simultaneous Growth of Multiple Hydraulic Fractures. *SPE Journal* **2015**, *20*, 384−395.
(19) Cipolla, C. L.; Lolon, E. P.; Mayerhofer, M. J.; Warpinski, N. R. The effect of proppant distribution and un-propped fracture conductivity on well performance in unconventional gas reservoirs. In SPE Hydraulic Fracturing Technology Conference (SPE 119368), 2009, The Woodlands, Texas.
(20) Siddhamshetty, P.; Liu, S.; Valkó, P. P.; Kwon, J. S. Feedback control of proppant bank heights during hydraulic fracturing for enhanced productivity in shale formations. *AIChE J.* **2018**, *64*, 1638−1650.
(21) Yang, S.; Siddhamshetty, P.; Kwon, J. S. Optimal pumping schedule design to achieve a uniform proppant concentration level in hydraulic fracturing. *Comput. Chem. Eng.* **2017**, *101*, 138−147.
(22) Siddhamshetty, P.; Wu, K.; Kwon, J. S. Optimization of simultaneously propagating multiple fractures in hydraulic fracturing to achieve uniform growth using data-based model reduction. *Chem. Eng. Res. Des.* **2018**, *136*, 675−686.
(23) Siddhamshetty, P.; Yang, S.; Kwon, J. S. Modeling of hydraulic fracturing and designing of online pumping schedules to achieve uniform proppant concentration in conventional oil reservoirs. *Comput. Chem. Eng.* **2018**, *114*, 306−317.
(24) Narasingam, A.; Siddhamshetty, P.; Kwon, J. S. Temporal clustering for order reduction of nonlinear parabolic PDE systems with time-dependent spatial domains: Application to a hydraulic fracturing process. *AIChE J.* **2017**, *63*, 3818−3831.
(25) Narasingam, A.; Siddhamshetty, P.; Kwon, J. S. Handling Spatial Heterogeneity in Reservoir Parameters Using Proper Orthogonal Decomposition Based Ensemble Kalman Filter for Model-Based Feedback Control of Hydraulic Fracturing. *Ind. Eng. Chem. Res.* **2018**, *57*, 3977−3989.
(26) Singh Sidhu, H.; Siddhamshetty, P.; Kwon, J. S. Approximate Dynamic Programming Based Control of Proppant Concentration in Hydraulic Fracturing. *Mathematics* **2018**, *6*, 132.
(27) Sidhu, H. S.; Narasingam, A.; Siddhamshetty, P.; Kwon, J. S. Model order reduction of nonlinear parabolic PDE systems with moving boundaries using sparse proper orthogonal decomposition: Application to hydraulic fracturing. *Comput. Chem. Eng.* **2018**, *112*, 92−100.
(28) Wu, K.; Olson, J. E. Simultaneous multifracture treatments: fully coupled fluid flow and fracture mechanics for horizontal wells. *SPE Journal* **2015**, *20*, 337−346.
(29) Crouch, S. L.; Starfield, A. M.; Rizzo, F. J. Boundary element methods in solid mechanics. *J. Appl. Mech.* **1983**, *50*, 704.
(30) Shou, K. A higher order three-dimensional displacement discontinuity method with application to bonded half-space problems. Ph.D. Thesis, University of Minnesota, Minneapolis, Minnesota, 1993.
(31) Elbel, J. L.; Piggott, A. R.; Mack, M. G. Numerical modeling of multilayer fracture treatments. In Permian Basin Oil and Gas Recovery Conference. Society of Petroleum Engineers (SPE 23982), 1992, Midland, Texas.
(32) Valko, P.; Economides, M. J. In *Hydraulic fracture mechanics*; Wiley: Chichester, 1995.
(33) Daneshy, A. Numerical solution of sand transport in hydraulic fracturing. *JPT, J. Pet. Technol.* **1978**, *30*, 132−140.
(34) Barree, R.; Conway, M. Experimental and numerical modeling of convective proppant transport. *JPT, J. Pet. Technol.* **1995**, *47*, 216−222.
(35) Adachi, J.; Siebrits, E.; Peirce, A.; Desroches, J. Computer simulation of hydraulic fractures. *International Journal of Rock Mechanics and Mining Sciences* **2007**, *44*, 739−757.
(36) Televantos, Y.; Shook, C.; Streat, M.; Carleton, A. Flow of slurries of coarse particles at high solids concentrations. *Can. J. Chem. Eng.* **1979**, *57*, 255−262.
(37) Liu, S.; Valkó, P. P. Optimization of spacing and penetration ratio for infinite conductivity fractures in unconventional reservoirs- A sectional based approach. *SPE Journal* **2017**, *22*, 1877−1892.
(38) Maxwell, S. C.; Rutledge, J.; Jones, R.; Fehler, M. Petroleum reservoir characterization using downhole microseismic monitoring. *Geophysics* **2010**, *75*, 75A129−75A137.
(39) Van Overschee, P.; De Moor, B. N4SID: Subspace algorithms for the identification of combined deterministic-stochastic systems. *Automatica* **1994**, *30*, 75−93.

DOI: 10.1021/acs.iecr.8b05654
Ind. Eng. Chem. Res. 2019, 58, 3159−3169